AGU ADVANCING EARTH AND SPACE SCIENCES

Geophysical Research Letters

RESEARCH LETTER
10.1029/2024GL111670

Poloidal Field Line Resonances Driven by a Fast Wave

Andrew Wright[1], Thomas Elsden[1], Alexander Degeling[2], Ian R. Mann[3], Louis Ozeke[3], Timothy Yeoman[4], Jasmine Sandhu[4], and Kazue Takahashi[5]

[1]School of Mathematics and Statistics, University of St Andrews, St Andrews, UK, [2]Shandong Provincial Key Laboratory of Optical Astronomy and Solar-Terrestrial Environment, Institute of Space Sciences, Shandong University, Weihai, China, [3]Department of Physics, University of Alberta, Edmonton, AB, Canada, [4]School of Physics and Astronomy, University of Leicester, Leicester, UK, [5]The Johns Hopkins University Applied Physics Laboratory, Laurel, MD, USA

Key Points:

- Resonant Poloidal Alfvén waves can be driven by a fast mode wave
- Classifying Field Line Resonances as high-*m* and low-*m* has limited applicability in 3D equilibria
- Phasemixing can occur in the toroidal direction

Supporting Information:

Supporting Information may be found in the online version of this article.

Correspondence to:

A. Wright,
anw@st-and.ac.uk

Citation:

Wright, A., Elsden, T., Degeling, A., Mann, I. R., Ozeke, L., Yeoman, T., et al. (2025). Poloidal field line resonances driven by a fast wave. *Geophysical Research Letters*, *52*, e2024GL111670. https://doi.org/10.1029/2024GL111670

Received 1 AUG 2024
Accepted 27 JAN 2025

Abstract We present numerical simulations of the excitation of resonant poloidal Alfvén waves. The resulting Alfvén waves could be loosely described as "high-*m*" (*m* is the azimuthal wave number) in as much as the azimuthal scale of the wave is much less than the scale in the direction normal to *L*-shells. Such waves are generally excited by wave-particle interactions. In this article we show how resonant poloidal Alfvén waves can be excited by a fast mode (of large azimuthal scale) in a cold plasma. The key property that enables this is a three-dimensional equilibrium, which facilitates the process of phasemixing in the azimuthal direction. We show that the classification of resonant Alfvén waves as high-*m* and low-*m* has limited applicability in 3D inhomogeneous media and suggest an alternative classification be based on the excitation mechanism.

Plain Language Summary The environment surrounding the Earth comprises plasma (an ionized gas) permeated by the terrestrial magnetic field. This medium can exhibit a range of global wave-like oscillations. Of particular interest are waves that stand along the entire length of a field line. Traditional modeling shows that when these waves are excited by a different (compressional) mode of oscillation, the field line is displaced in the azimuthal direction. Here we use computer simulations to show that when this process occurs in a 3D medium, the plasma displacement can be directed at 90° to the traditional direction. This will allow for the wave to interact strongly with charged particles trapped in the Earth's magnetic field so has important consequences for understanding Space Weather.

1. Introduction

Resonantly driven Alfvén waves, also known as Field Line Resonances (FLRs), are common in the Earth's magnetosphere (see A. N. Wright et al. (2024) and references therein). Traditionally FLRs have been considered in a 1D or 2D regime, and they are classified as either "high-*m*" or "low-*m*," where *m* is the azimuthal wave-number. High-*m* FLRs are polarized to have the plasma displacement in a meridional plane (poloidal), whilst low-*m* FLRs have an azimuthal (toroidal) polarisation (Dungey, 1954). Low-*m* FLRs are excited by resonant coupling with the fast mode (Allan et al., 1986; Kivelson & Southwood, 1986; Lee & Lysak, 1989; Southwood, 1974; A. N. Wright & Thompson, 1994; A. N. Wright & Rickard, 1995). High-*m* FLRs are driven by wave-particle interactions (Chen & Hasegawa, 1991; Hughes et al., 1978; James et al., 2013; Ozeke & Mann, 2001; Southwood, 1976; Yeoman & Wright, 2001).

"Poloidal" and "toroidal" Alfvenic wave polarizations continue to be associated with waves with transverse plasma displacement in the radial and azimuthal directions in the magnetosphere, as would be inferred in an axisymmetric background equilibrium. However, the nature of 3-D wave coupling requires that these wave mode polarizations are distorted in non-axisymmetric plasma configurations—such that any polarisation is possible. As we show here, this means fro example that the resulting Alfvenic waves can have a "poloidal" polarisation even when driven by large scale "low-m" fast mode waves.

Recently the process of resonant fast-Alfvén wave coupling in 3D equilibria has been studied (Degeling et al., 2018; Degeling et al., 2018; A. N. Wright & Elsden, 2016). Reviews of this topic include Elsden et al. (2022) and A. N. Wright et al. (2024). In 3D the polarisation of the Alfvén wave is no longer strictly toroidal and this will occur in any equilibrium that is not axisymmetric, such as when there is a partial ring current or substorm activity. For example, if the equilibrium contains a plasmaspheric plume, simulations show the FLR polarisation can lie between the toroidal and poloidal limits (Elsden & Wright, 2022; A. N. Wright &

Elsden, 2020). Indeed, Sandhu et al. (2023) have confirmed this property is observed in satellite transits of plume boundaries. The results we present in this paper go even further and show fast mode driven FLRs can have a polarisation that is completely poloidal.

In this article we question the assumption that poloidal FLRs must be driven by wave-particle interactions. We present simulation results that show a 3D equilibrium can permit phasemixing in the azimuthal direction. This leads to a poloidally polarized FLR that is driven via coupling with the fast mode, rather than via wave-particle interactions, and is contrary to the commonly accepted view.

2. Simulation Details and Key 3D FLR Concepts

The numerical model is described in detail in A. N. Wright and Elsden (2020), but we summarize the key features here for convenience. The simulation uses a dipole equilibrium magnetic field on which a field aligned coordinate system is based. The time-dependent linearized cold plasma equations are solved for the magnetic field and velocity perturbations. The plasma density (and hence Alfvén speed) is a general function of position, so the solutions represent wave propagation and coupling in a 3D equilibrium. The simulation starts with no perturbations present, and is then driven by applying a magnetic pressure perturbation on the magnetopause. For simplicity, we take the magnetopause to be given by the $L = 10$ magnetic surface. (L is the L-shell parameter).

For numerical convenience we take the Alfvén speed to be constant along a field line, but it can be an arbitrary function of L and magnetic local time (MLT). To illustrate the 3D nature of the solutions we introduce a density enhancement in the afternoon which mimics the presence of a plasmaspheric plume. This leads to a local lowering of the Alfvén speed and Alfvén frequencies. The resulting variation of toroidal $\left(f_{AT}\right)$ and poloidal $\left(f_{AP}\right)$ Alfvén frequencies are displayed in the equatorial plane in the afternoon quadrant in Figures 1a and 1b. The Alfvén frequencies are calculated by solving the toroidal and poloidal eigenfrequency equations (see, for example, Equations 3 and 4 of Elsden et al. (2022)). These equations are solved using the shooting method for perfectly conducting ionospheres.

The Alfvén speed variation is taken to be axisymmetric away from the plume, which is centered on 15 hr MLT and has a width of 2 hr in MLT. Figure 1c shows the variation of toroidal and poloidal Alfvén frequencies with L away from the plume (e.g., at noon and dusk), whilst Figure 1d shows their dependence on L at 15 MLT through the center of the plume. Panel (e) shows the frequency variation with MLT on $L = 7.75$.

It is well known that in a dipole field the toroidal and poloidal Alfvén frequencies are different (Dungey, 1954; Radoski, 1967). (Here, the Alfvén wave polarisation corresponds to the direction of the Alfvén wave plasma displacement in the equatorial plane). Toroidal and poloidal polarizations are two possible limiting values, but in 3D equilibria any intermediate polarisation could occur. In a dipole equilibrium the maximum Alfvén frequency on a given field line is always the toroidal frequency and the minimum is the poloidal frequency. A. N. Wright and Elsden (2016) show how an Alfvén wave with a polarisation between toroidal and poloidal will have an Alfvén frequency between the toroidal and poloidal frequencies. They also introduced the concept of a Resonant Zone, which corresponds to the region where it is possible to find a polarisation such that the Alfvén frequency matches a given driving frequency, that is, where it is possible for an FLR to occur.

For example, if the equilibrium is driven at a frequency of $f_d = 2$ mHz the horizontal black lines in Figures 1c, 1d, and 1e can be used to identify the Resonant Zone. At 15 MLT panel (d) shows that $f_{AP} < f_d < f_{AT}$ for any $L > 5.4$. At noon and dusk panel (c) shows that $f_{AP} < f_d < f_{AT}$ for $5.4 < L < 6.5$ and for $L > 9.0$. Importantly, for $6.5 < L < 9.0$ it is not possible for the Alfvén frequency (for any polarisation) to match f_d, so this region forms part of the Non-Resonant Zone. On the $L = 7.75$ surface panel (e) shows that $14 <$ MLT < 16 will be in the Resonant Zone, whilst other MLTs will contain non-resonant field lines. Repeating this analysis for all L and MLT allows us to plot the Resonant Zone boundaries shown in panel (f). The Resonant Zone is the region centered on $(X, Y) = (6, 6)$ and bounded by the magnetopause and the red lines (which correspond to where $f_{AP} = f_d$). We note that for this particular equilibrium and choice of f_d it is not possible to satisfy $f_{AT} = f_d$ (the black and blue lines in Figures 1c, 1d, and 1e do not intersect).

The simulation is driven by applying a magnetic pressure perturbation on the magnetopause (see Section 3). For computational efficiency, we focus on the afternoon quadrant. The simulation domain extends a little before 12 MLT and a little after 18 MLT where buffer zones cause dissipation (via a drag term) of any waves arriving

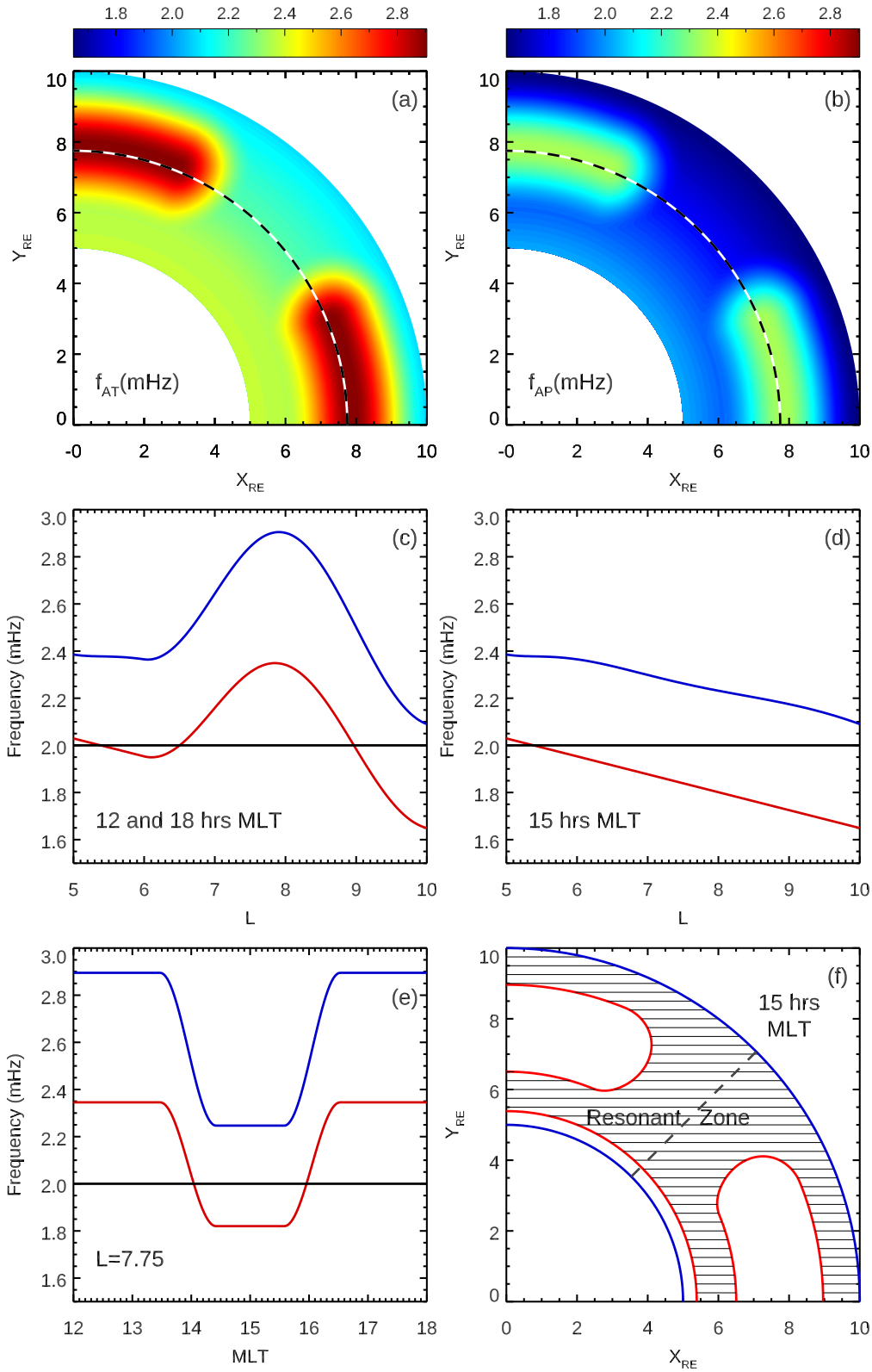

Figure 1. Variation of the (a) toroidal and (b) poloidal Alfvén frequencies in the equatorial plane in the afternoon quadrant. The dashed line is at $L = 7.75$. (c) Variation of the frequencies (blue-toroidal, and red-poloidal) with L at noon and/or dusk and (d) through the center of the plume at 15 hr MLT. (e) Frequency variation with MLT through the center of plume ($L = 7.75$). (f) Resonant Zone Boundaries for a driving freq of 2 mHz where $f_{AP} = f_d$ (red) and simulation boundaries (blue) in the equatorial plane.

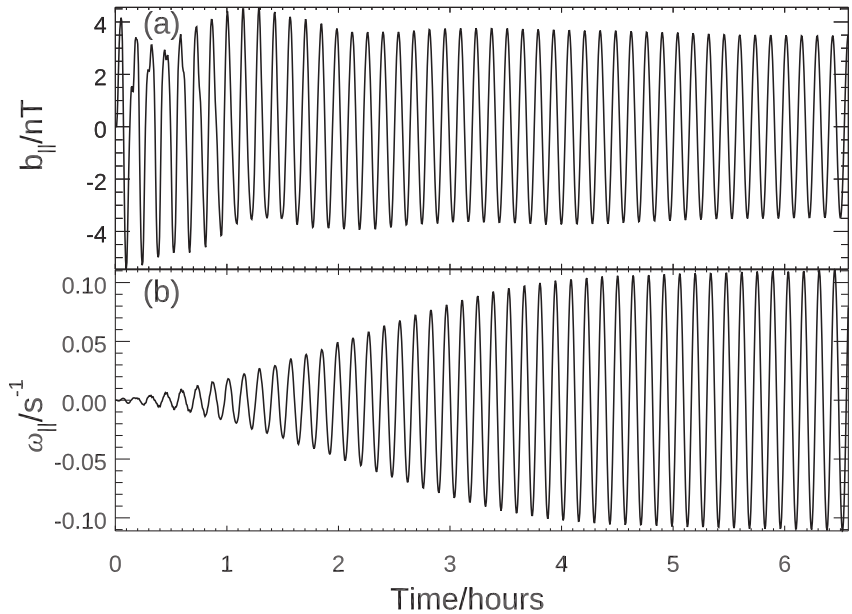

Figure 2. (a) The variation of $b_{||}$ with time in the equatorial plane at (5.3,5.3), and (b) $\omega_{||}$ versus time at (6.7,3.9).

there. This mimics the loss of waves across noon to the dawn flank and also into the tail via the dusk flank. The inner boundary at $L = 5$ is perfectly reflecting.

3. Simulation Results

To stress that it is possible for poloidal Alfvén waves to be driven by a low azimuthal wave number (m) fast mode wave, we apply an $m = 0$ magnetic pressure driver on the magnetopause corresponding to a compressional magnetic field of 5 nT in the equatorial plane which oscillates monochromatically with a frequency of 2 mHz. The driver decreases to zero symmetrically away from the equatorial plane along the field lines on the magnetopause with a length scale of 5.5 R_E. Figure 2a shows the variation of the compressional magnetic field at $L = 7.5$ and 15 MLT (equivalent to $X = Y = 5.3$). The 2 mHz driving frequency is evident. Panel (b) shows the field-aligned vorticity $(\omega_{||})$ in the equatorial plane at the point $(X, Y) = (6.7, 3.9)$ (or $L = 7.75$ and MLT = 14 hr). We note that $b_{||}$ is zero in an Alfvén wave but nonzero in a fast wave. In contrast the field-aligned vorticity $\omega_{||} = (\nabla \times \boldsymbol{u})_{||}$ is zero in a fast wave but nonzero in an Alfven wave ($\boldsymbol{u}$ is the plasma velocity). Thus $b_{||}$ and $\omega_{||}$ allow us to identify where the fast and Alfvén waves are located.

Figure 2a shows how the fast mode has strong transients over the first hour, but settles down to a steady oscillation after 2 hours due to dissipation in the buffer zones. The vorticity takes longer to saturate. This is because once the fast mode has settled down to providing a monochromatic driver the FLR needs to grow to an amplitude where the energy absorbed from the fast mode is balanced by resistive dissipation in the FLR. This is achieved by having a small value of resistivity present (A. N. Wright & Elsden, 2020) which determines the width and amplitude of the Alfvén wave (A. N. Wright & Allan, 1996).

Although the behavior of waves in the Earth's magnetosphere is generally dynamic and will exhibit significant transient characteristics, a sound mathematical understanding and much physical insight can be gained from normal mode solutions (i.e., waves with a steady monochromatic oscillatory nature). For this reason we focus on the waves near the end of the simulation run. Elsden and Wright (2018) show how two simulation snapshots taken a quarter of a cycle apart can correspond to the real and imaginary parts of a complex normal mode (i.e., all wave fields vary proportional to $\exp(i2\pi f_d t)$). Such snapshots are shown in Figure 3. Panels (a) and (b) show the structure of the fast normal mode in the equatorial plane $(b_{||})$, whilst (c) and (d) show the structure of the FLR via the field-aligned vorticity $(\omega_{||})$. The fast mode extends over the entire domain. In contrast, the FLR is mainly excited on two specific surfaces of resonant field lines that extend from the magnetopause deep into the magnetosphere. The spatial structure of the fast mode shown in Figures 3a and 3b is particularly important as the

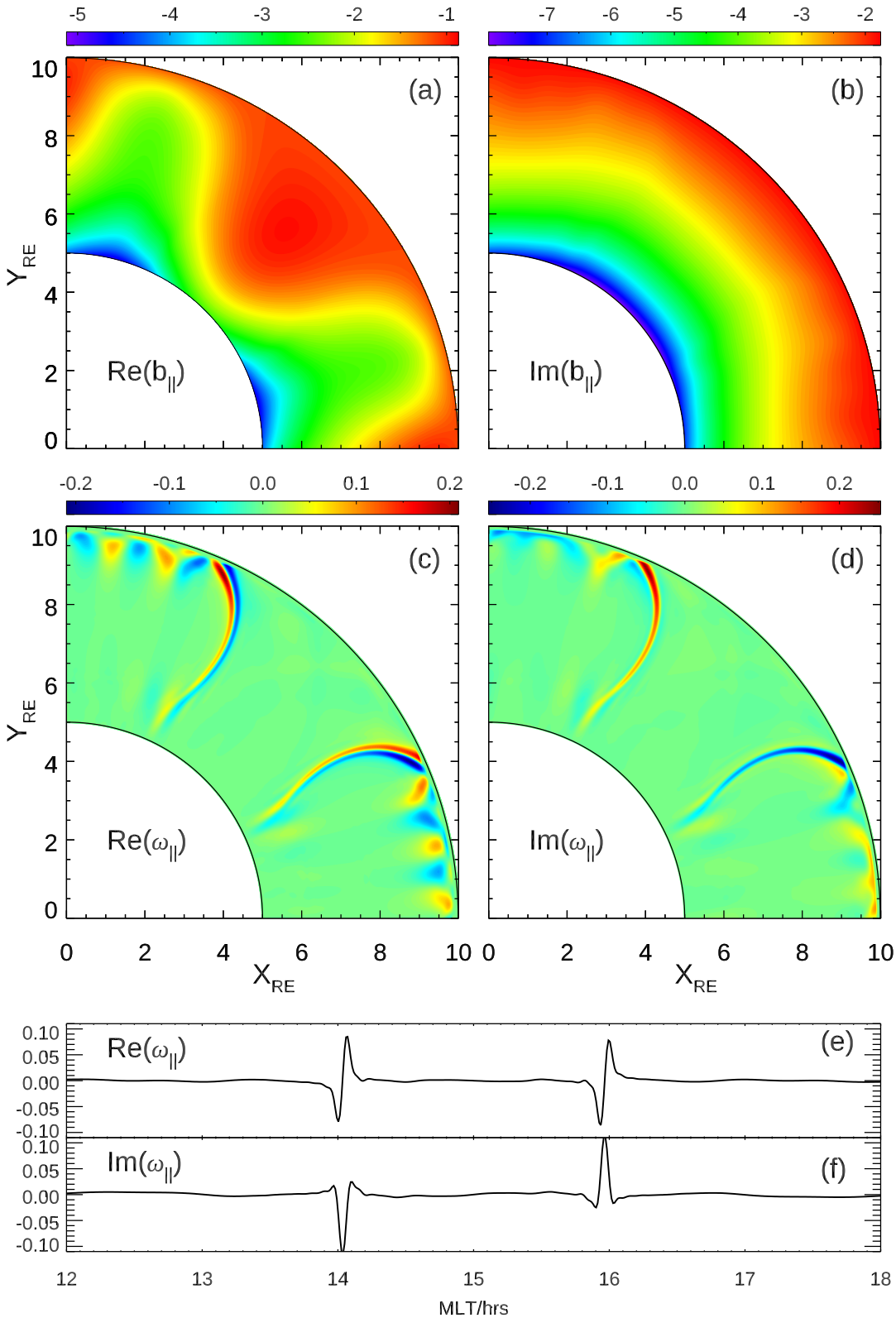

Figure 3. Normal mode structure for a frequency of 2 mHz: The variation in the equatorial plane of the real (a) and imaginary (b) parts of $b_{\parallel}$ (nT). The real (c) and imaginary (d) parts of $\omega_{\parallel}$ (s^{-1}). Real (e) and imaginary (f) parts of $\omega_{\parallel}$ versus MLT ($L = 7.75$).

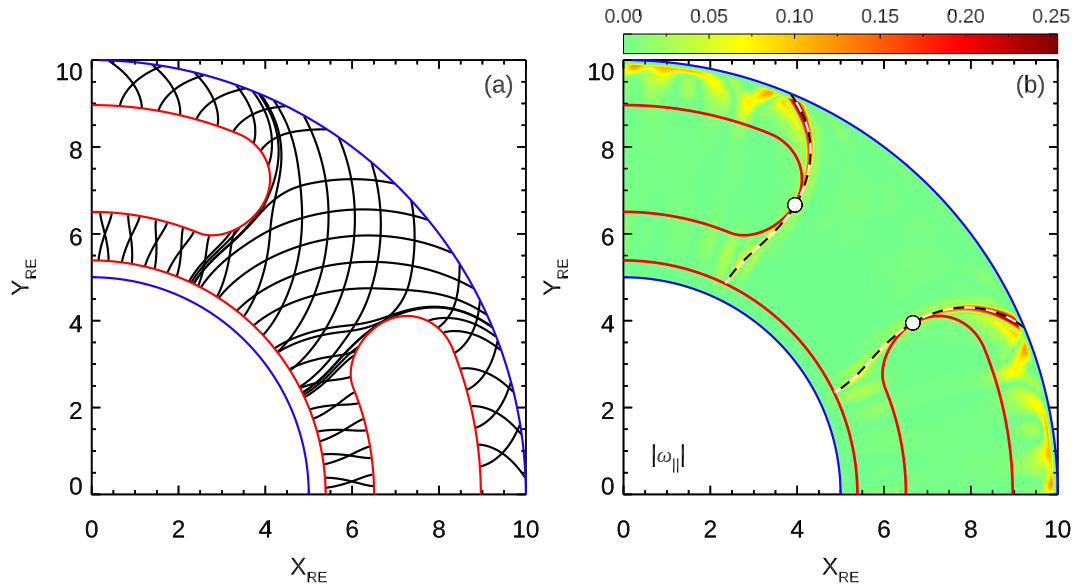

Figure 4. (a) The Resonance Map for $f_d = 2$ mHz. Blue lines indicate the simulation boundaries. Red lines are the Resonant Zone Boundaries, and black lines the permissible resonant paths. (b) A comparison of the FLR structure ($|\omega_{||}|/s^{-1}$) with the Resonance Map. The white dots indicate points where the Tangential Alignment condition is satisfied, and the dashed black lines are the resonant paths through these points.

force that drives the Alfvén wave equation is the fast mode magnetic pressure gradient, which is proportional to $b_{||}$ (Elsden & Wright, 2017).

The FLR fields are highly localized perpendicular to the resonant surfaces. This can be seen clearly in panels (e) and (f) which show the variation of $\omega_{||}$ with MLT on the $L = 7.75$ shell in the equatorial plane. Evidently the Alfvén waves are centered on ∼14 and ∼16 hr MLT. A. N. Wright and Elsden (2016) show that the FLR plasma velocity is tangential to the resonant surfaces that are evident in panels (c) and (d). (It is the derivative of this velocity across the resonant surface that produces $\omega_{||}$). Hence, the FLRs produced have a polarisation that is predominantly poloidal.

Figure 3 shows the narrow saturated width of the FLR in MLT. At earlier times the width is broader and may be estimated from the azimuthal phasemixing scale of the poloidal Alfvén wave, $L_{ph} \propto 1/t$ (Mann et al., 1995). In the Supporting Information S1 we include a movie of $b_{||}$ and $\omega_{||}$ as well as two snapshots of the azimuthal variation of $\omega_{||}$ from which it is clear that the FLR narrows in width and grows in amplitude until it reaches the saturated normal mode structure in Figure 3.

4. Discussion and Concluding Remarks

The Resonant Zone boundaries, shown in Figure 1f are reproduced in Figure 4a as the red lines. The black lines represent the intersection of possible FLR resonant surfaces with the equatorial plane: the FLRs would have their plasma displacement tangential to the black lines, and for this polarisation the Alfvén frequency will match f_d (A. N. Wright & Elsden, 2016), hence these lines are referred to as resonant paths. It is evident that where the resonant paths intersect the red lines, they have a poloidal orientation, which is to be expected as the red lines were defined to be the points where $f_{AP} = f_d$. As the resonant paths move away from the red boundaries their orientation turns to adopt a polarisation that lies between the poloidal and toroidal directions. It is interesting to note that the resonant paths have also been derived from a theoretical standpoint by Leonovich and Mazur (1993) and Klimushkin et al. (1995) who showed the paths are contours of asymptotic phase. They also noted that the perpendicular group velocity of the Alfvén waves is directed along these paths—a property which has been observed in the simulations of Elsden and Wright (2020).

It is clear from Figure 4a that there are an infinite number of possible resonant paths (only representative ones are shown here), and it is equally clear from Figures 3c and 3d that two particular resonant paths dominate the FLR

response. The magnitude of FLR vorticity in Figures 3c and 3d is shown in Figure 4b along with the simulation boundaries (blue), the Resonant Zone boundaries (red) and the two favored resonant paths (black dash). A. Wright et al. (2022) note these paths can be determined using the Tangential Alignment Condition: identify the points on the Resonant Zone boundary where the resonant paths are tangential to the boundary (see the white dots in Figure 4b). Such locations are referred to as Tangential Alignment Points, and it is the resonant paths passing through these points that are favored. A. N. Wright (2023) showed these points can also be determined from a minimization principle.

Whilst the Tangential Alignment Condition works well for our results, it should be noted that some details are not accounted for. For example, the Tangential Alignment Point at 14 hr MLT (or $(X, Y) = (6.7, 3.9)$) has an FLR on the path that turns toward noon as it approaches the magnetopause. However, the Resonance Map in Figure 4a shows there is another resonant path through this point that turns toward dusk as it approaches the magnetopause, yet there is no FLR present on this path. It is not clear why one path is favored over the other. Elsden and Wright (2017) show how the amplitude of an FLR is governed by the magnetic pressure gradient along the resonant path, so this might provide some explanation. The question is certainly worthy of more study.

The traditional classification of FLRs has been in terms of azimuthal wavenumber, m: low-m FLRs have a toroidal polarisation and are driven by magnetic pressure gradients of the fast mode; high-m FLRs have a poloidal polarisation and are driven by wave-particle interactions. Limitations of these classifications have become highlighted by studies in 3D which show that FLRs can have a polarisation that is intermediate to the toroidal and poloidal limits (Degeling et al., 2018; Elsden et al., 2022; A. N. Wright & Elsden, 2016, 2024). The results we report in this article highlight a further limitation of the traditional classification, namely that poloidal FLRs can be driven by fast mode pressure gradients. We suggest FLRs should be classified solely by their generation mechanism since there is considerable variablility over permissible polarizations. Hence, we refer to the FLRs reported here as "fast mode-driven" FLRs which, in this instance, have a poloidal polarisation. (In a different equilibrium, the polarisation could change). The other type of FLR can be termed "particle-driven." We note that for FLRs with intermediate values of m either driving mechanism may operate: particle-driven FLRs have been reported by Yeoman et al. (2010) ($m = 13$), and by Mager et al. (2019) ($m = -10$). Yet similar wavenumber FLRs ($m = 14$) can be driven by MHD waves associated with an interplanetary shock (Hao et al., 2014).

It is interesting to consider how the traditional classification came into existence, and why it is no longer considered to be accurate. For particle driven FLRs, the value of m is determined by a bounce/drift resonance condition (Dai et al., 2013; Southwood et al., 1969; Southwood & Kivelson, 1981, 1982; Takahashi et al., 2013), and for typical parameters at Earth the resulting value of m is high. A high-m FLR will naturally have a poloidal polarisation—hence the identification between particle-driven, high-m and poloidal polarisation. Of course, if particle drift frequencies and Alfvén frequencies were to change, it could be possible to have lower m particle-driven FLRs, and the polarisation would no longer be poloidal.

The FLRs driven by fast mode waves have been modeled extensively in 1D and 2D axisymmetric equilibria where it is permissible to consider azimuthal Fourier modes (m) independently. The matching of fast and Alfvén frequencies occurs in the evanescent tail of the fast mode (Southwood, 1974; A. N. Wright, 1994). As m increases the fast mode becomes more evanescent, and the energy coupled to the resonant FLR becomes negligible. Hence, it is not thought to be possible to drive a high-m FLR by the fast mode. The optimum coupling between the fast mode and an FLR occurs for a low value of m (Kivelson & Southwood, 1986): when m is low, the FLR lies just a little way into the evanescent tail of the fast mode, so the fast mode has not decayed significantly. Also, a non-zero value of m means there will be pressure gradients in the azimuthal direction to drive the FLR. Indeed, theory confirms that such FLRs will have a toroidal polarisation (Southwood, 1974; A. N. Wright & Thompson, 1994), hence the correlation between fast mode driving, low-m values and toroidal polarisation.

The reason the above traditional classification does not suit the FLRs we report here is because our equilibrium is not axisymmetric. A consequence of this is that we cannot consider the azimuthal Fourier modes (m) to be decoupled from one another, so we cannot consider one value of m to be a reasonable approximation to a physical solution. The 3D nature of our equilibrium means that Alfvén frequencies will vary with local time (e.g., Figure 1e) which leads to behavior that is not possible in an axisymmetric equilibrium. From a time-dependent perspective, an initial nudge of the field lines may give rise to phasemixing in the toroidal direction. Adapting the traditional formula for the ideal phasemixing length in the poloidal direction (Mann et al., 1995) we find the toroidal phasemixing length is

$$L_{ph} = \frac{1}{(\mathbf{e}_\phi \cdot \nabla f_{AP})\, t}, \quad (1)$$

where $\mathbf{e}_\phi$ is the unit vector in the azimuthal direction.

As the azimuthal phasemixing length becomes smaller than the radial extent of the FLR, the phasemixing Alfvén waves will naturally adopt a poloidal polarisation. For suitable frequency gradients and FLR lifetimes (governed by dissipation) it is possible to drive these poloidal Alfvén waves resonantly by fast mode pressure gradients, as we see in our simulation. If our equilibrium did not vary in azimuth, phasemixing in the azimuthal direction would not occur, and we could not drive a poloidal FLR by this mechanism.

In summary, the traditional classification of high-*m* and low-*m* FLRs and their properties are based on normal modes in axisymmetric equilibria. In 3D, these modes have limited applicability and cannot describe the more general behavior that is possible in a 3D equilibrium. We suggest it is more accurate to simply classify the possible FLRs as "fast mode-driven" and "particle-driven." Additional properties, such as polarisation, vary considerably from one instance to another, so polarisation is not a reliable indicator of the physics operating.

Our results highlight the importance of realistic modeling of wave properties in 3D equilibria. Fast mode waves can couple to FLRs with unusual properties, and our results show these may have a poloidal polarisation and small scale in the azimuthal direction. Such FLRs are known to interact strongly with trapped particles. Indeed, the commonly accepted view is that such FLRs are excited at the expense of energy in unstable particle distributions. Here we raise the possibility that the FLRs can derive their energy from the fast mode. Once established we would anticipate a strong interaction with trapped particles, probably energizing them and causing diffusion across *L* shells.

Data Availability Statement

Data used to make the simulation figures in this paper can be found in (A. N. Wright, 2025).

Acknowledgments
This research was supported by the International Space Science Institute (ISSI) in Bern, through ISSI International Team project #483 (The Identification and Classification of 3D Alfvén Resonances). The authors are grateful to ISSI for funding the Team and hosting its meetings. ANW was partially funded by the Science and Technology Facilities Council (STFC) Grant (ST/N000609/1). KT was supported by NASA 80NSSC19K0259. JKS was funded by STFC Grant ST/W00089X/1. AWD is funded by NSFC (RFIS-III Grant 42350710200). TKY acknowledges support from STFC UKRI Grant ST/W00089X/1 and NERC UKRI Grant NE/V000748/1. LO and IRM were supported by funding from the Canadian Space Agency. IRM was also funded by a Discovery Grant from the Canadian NSERC.

References

Allan, W., Poulter, E. M., & White, S. P. (1986). Hydromagnetic wave coupling in the magnetosphere—Plasmapause effects on impulse-excited resonances. *Planetary and Space Science*, *34*(12), 1189–1200. https://doi.org/10.1016/0032-0633(86)90056-5

Chen, L., & Hasegawa, A. (1991). Kinetic-theory of geomagnetic-pulsations .1. Internal excitations by energetic particles. *Journal of Geophysical Research*, *96*(A2), 1503–1512. https://doi.org/10.1029/90ja02346

Dai, L., Takahashi, K., Wygant, J. R., Chen, L., Bonnell, J., Cattell, C. A., et al. (2013). Excitation of poloidal standing Alfvén waves through drift resonance wave-particle interaction. *Geophysical Research Letters*, *40*(16), 4127–4132. https://doi.org/10.1002/grl.50800

Degeling, A. W., Rae, I. J., Watt, C. E. J., Shi, Q. Q., Rankin, R., & Zong, Q. G. (2018). Control of ULF wave accessibility to the inner magnetosphere by the convection of plasma density. *Journal of Geophysical Research: Space Physics*, *123*(2), 1086–1099. https://doi.org/10.1002/2017JA024874

Dungey, J. W. (1954). *Electrodynamics of the outer atmosphere: Report to national science foundation on work carried on under grant NSF-g450*. Pennsylvania State University, Ionosphere Research Laboratory. Retrieved from https://books.google.co.uk/books?id=3NrUAAAAMAAJ

Elsden, T., Wright, A., & Degeling, A. (2022). A review of the theory of 3-D Alfvén (field line) resonances. *Frontiers in Astronomy and Space Sciences*, *9*, 917817. https://doi.org/10.3389/fspas.2022.917817

Elsden, T., & Wright, A. N. (2017). The theoretical foundation of 3-D Alfvén resonances: Time-dependent solutions. *Journal of Geophysical Research: Space Physics*, *122*(3), 3247–3261. https://doi.org/10.1002/2016JA023811

Elsden, T., & Wright, A. N. (2018). The broadband excitation of 3-D Alfvén resonances in a MHD waveguide. *Journal of Geophysical Research: Space Physics*, *123*(1), 530–547. https://doi.org/10.1002/2017JA025018

Elsden, T., & Wright, A. N. (2020). Evolution of high-m poloidal Alfvén waves in a dipole magnetic field. *Journal of Geophysical Research: Space Physics*, *125*(8), e28187. https://doi.org/10.1029/2020JA028187

Elsden, T., & Wright, A. N. (2022). Polarization properties of 3-D field line resonances. *Journal of Geophysical Research: Space Physics*, *127*(2), e30080. https://doi.org/10.1029/2021JA030080

Hao, Y. X., Zong, Q. G., Wang, Y. F., Zhou, X. Z., Zhang, H., Fu, S. Y., et al. (2014). Interactions of energetic electrons with ULF waves triggered by interplanetary shock: Van Allen Probes observations in the magnetotail. *Journal of Geophysical Research: Space Physics*, *119*(10), 8262–8273. https://doi.org/10.1002/2014JA020023

Hughes, W. J., Southwood, D. J., Mauk, B., McPherron, R. L., & Barfield, J. N. (1978). Alfven waves generated by an inverted plasma energy distribution. *Nature*, *275*(5675), 43–45. https://doi.org/10.1038/275043a0

James, M. K., Yeoman, T. K., Mager, P. N., & Klimushkin, D. Y. (2013). The spatio-temporal characteristics of ULF waves driven by substorm injected particles. *Journal of Geophysical Research: Space Physics*, *118*(4), 1737–1749. https://doi.org/10.1002/jgra.50131

Kivelson, M. G., & Southwood, D. J. (1986). Coupling of global magnetospheric MHD eigenmodes to field line resonances. *Journal of Geophysical Research*, *91*(A4), 4345–4351. https://doi.org/10.1029/JA091iA04p04345

Klimushkin, D. Y., Leonovich, A. S., & Mazur, V. A. (1995). On the propagation of transversally small-scale standing Alfven waves in a three-dimensionally inhomogeneous magnetosphere. *Journal of Geophysical Research*, *100*(A6), 9527–9534. https://doi.org/10.1029/94JA03233

Lee, D.-H., & Lysak, R. L. (1989). Magnetospheric ULF wave coupling in the dipole model - The impulsive excitation. *Journal of Geophysical Research*, *94*, 17097–17103. https://doi.org/10.1029/JA094iA12p17097

Leonovich, A. S., & Mazur, V. A. (1993). A theory of transverse small-scale standing Alfvén waves in an axially symmetric magnetosphere. *Planetary and Space Science*, *41*(9), 697–717. https://doi.org/10.1016/0032-0633(93)90055-7

Mager, O. V., Chelpanov, M. A., Mager, P. N., Klimushkin, D. Y., & Berngardt, O. I. (2019). Conjugate ionosphere-magnetosphere observations of a sub-Alfvénic compressional intermediate-m wave: A case study using EKB radar and Van Allen Probes. *Journal of Geophysical Research: Space Physics*, *124*(5), 3276–3290. https://doi.org/10.1029/2019JA026541

Mann, I. R., Wright, A. N., & Cally, P. S. (1995). Coupling of magnetospheric cavity modes to field line resonances: A study of resonance widths. *Journal of Geophysical Research*, *100*(A10), 19441–19456. https://doi.org/10.1029/95JA00820

Ozeke, L. G., & Mann, I. R. (2001). Modeling the properties of high-m Alfvén waves driven by the drift-bounce resonance mechanism. *Journal of Geophysical Research*, *106*(A8), 15583–15598. https://doi.org/10.1029/2000JA000393

Radoski, H. R. (1967). A note on oscillating field lines. *Journal of Geophysical Research*, *72*(1), 418–419. https://doi.org/10.1029/JZ072i001p00418

Sandhu, J. K., Degeling, A. W., Elsden, T., Murphy, K. R., Rae, I. J., Wright, A. N., et al. (2023). Van Allen Probes observations of a three-dimensional field line resonance at a plasmaspheric plume. *Geophysical Research Letters*, *50*(23), e2023GL106715. https://doi.org/10.1029/2023GL106715

Southwood, D. J. (1974). Some features of field line resonances in the magnetosphere. *Planetary Space Science*, *22*(3), 483–491. https://doi.org/10.1016/0032-0633(74)90078-6

Southwood, D. J. (1976). A general approach to low-frequency instability in the ring current plasma. *Journal of Geophysical Research*, *81*(19), 3340–3348. https://doi.org/10.1029/JA081i019p03340

Southwood, D. J., Dungey, J. W., & Etherington, R. J. (1969). Bounce resonant interaction between pulsations and trapped particles. *Planetary and Space Science*, *17*(3), 349–361. https://doi.org/10.1016/0032-0633(69)90068-3

Southwood, D. J., & Kivelson, M. G. (1981). Charged particle behavior in low-frequency geomagnetic pulsations 1. Transverse waves. *Journal of Geophysical Research*, *86*(A7), 5643–5655. https://doi.org/10.1029/JA086iA07p05643

Southwood, D. J., & Kivelson, M. G. (1982). Charged particle behavior in low-frequency geomagnetic pulsations 2. Graphical approach. *Journal of Geophysical Research*, *87*(A3), 1707–1710. https://doi.org/10.1029/JA087iA03p01707

Takahashi, K., Hartinger, M. D., Angelopoulos, V., Glassmeier, K.-H., & Singer, H. J. (2013). Multispacecraft observations of fundamental poloidal waves without ground magnetic signatures. *Journal of Geophysical Research: Space Physics*, *118*(7), 4319–4334. https://doi.org/10.1002/jgra.50405

Wright, A., Degeling, A. W., & Elsden, T. (2022). Resonance maps for 3D Alfvén waves in a compressed dipole field. *Journal of Geophysical Research: Space Physics*, *127*(4), e30294. https://doi.org/10.1029/2022JA030294

Wright, A. N. (1994). Dispersion and wave coupling in inhomogeneous MHD waveguides. *Journal of Geophysical Research*, *99*(A1), 159–167. https://doi.org/10.1029/93JA02206

Wright, A. N. (2023). Efficient resonant fast-Alfvén wave coupling as a minimization principle. *Journal of Geophysical Research: Space Physics*, *128*(12), e2023JA031779. https://doi.org/10.1029/2023JA031779

Wright, A. N. (2025). Poloidal field line resonances driven by a fast wave, (run15) [Dataset]. *Figshare*. https://doi.org/10.6084/m9.figshare.26379442.v1

Wright, A. N., & Allan, W. (1996). Structure, phase motion, and heating within Alfvén resonances. *Journal of Geophysical Research*, *101*(A8), 17399–17408. https://doi.org/10.1029/96JA01141

Wright, A. N., & Elsden, T. (2016). The theoretical foundation of 3D Alfvén resonances: Normal modes. *Astrophysical Journal*, *833*(2), 230. https://doi.org/10.3847/1538-4357/833/2/230

Wright, A. N., & Elsden, T. (2020). Simulations of MHD wave propagation and coupling in a 3-D magnetosphere. *Journal of Geophysical Research: Space Physics*, *125*(2), e27589. https://doi.org/10.1029/2019JA027589

Wright, A. N., Hartinger, M. D., Takahashi, K., & Elsden, T. (2024). Alfvén waves in the Earth's magnetosphere. *Geophysical Monograph Series*, *285*, 215–247. https://doi.org/10.1002/9781394195985.ch10

Wright, A. N., & Rickard, G. J. (1995). A numerical study of resonant absorption in a magnetohydrodynamic cavity driven by a broadband spectrum. *Astrophysical Journal*, *444*, 458–470. https://doi.org/10.1086/175620

Wright, A. N., & Thompson, M. J. (1994). Analytical treatment of Alfvén resonances and singularities in nonuniform magnetoplasmas. *Physics of Plasmas*, *1*(3), 691–705. https://doi.org/10.1063/1.870815

Yeoman, T. K., Klimushkin, D. Y., & Mager, P. N. (2010). Intermediate-m ULF waves generated by substorm injection: A case study. *Annales Geophysicae*, *28*(8), 1499–1509. https://doi.org/10.5194/angeo-28-1499-2010

Yeoman, T. K., & Wright, D. M. (2001). ULF waves with drift resonance and drift-bounce resonance energy sources as observed in artificially-induced HF radar backscatter. *Annales Geophysicae*, *19*(2), 159–170. https://doi.org/10.5194/angeo-19-159-2001